

The influence of binary stars on the kinematics of low-mass galaxies

S. De Rijcke^{1,2,*} and H. Dejonghe²

¹ *Current address : Astronomisches Institut, Universität Basel, Venusstrasse 7, 4102 Binningen, Switzerland*

² *Sterrenkundig Observatorium, Ghent University, Krijgslaan 281, S9, 9000 Gent, Belgium*

* *Postdoctoral Fellow of the Fund for Scientific Research - Flanders (Belgium)(F.W.O)*

sven.derijcke@rug.ac.be

herwig.dejonghe@rug.ac.be

25 October 2018

ABSTRACT

In this paper, the influence of binary stars on the measured kinematics of dwarf galaxies is investigated. Using realistic distributions of the orbital parameters (semi-major axis, eccentricity, ...), analytical expressions are derived for the changes induced by the presence of binary stars in the measured velocity moments of low-mass galaxies (such as the projected velocity dispersion and the 4th order Gauss-Hermite coefficient h_4). It is shown that there is a noticeable change in the observed velocity dispersion if the intrinsic velocity dispersion of a galaxy is of the same order as the binary velocity dispersion. The kurtosis of the line-of-sight velocity distribution (LOSVD) is affected even at higher values of the intrinsic velocity dispersion.

Moreover, the LOSVD of the binary stars (i.e. the probability of finding a star in a binary system with a particular projected velocity) is given in closed form, approximating the constituent stars of all binaries to revolve on circular orbits around each other. With this binary LOSVD, we calculate the observed LOSVD, the latter quantifying the movement of stars along the line of sight caused both by the stars' orbits through the galaxy and by the motion of stars in binary systems. As suggested by the changes induced in the moments, the observed LOSVD becomes more peaked around zero velocity and develops broader high-velocity wings. These results are important in interpreting kinematics derived from integrated-light spectra of low-mass galaxies and many of the intermediate results are useful for comparison with Monte Carlo simulations.

1 INTRODUCTION

The usual approach to derive the kinematics (mean velocity along the line of sight, the velocity dispersion, ...) of galaxies from observed spectra is comparing them to the spectra of so-called template stars. The broadening of the absorption lines in the galaxy spectra is then interpreted as a result of the orbital motion of the myriad of stars along the line of sight through the galaxy : each star has a Doppler shifted spectrum and the absorption lines consequently appear at slightly different wavelengths. These template stars are carefully selected : they should not rotate too rapidly, not be member of a binary system or be peculiar in any other way so as to be a good representation of the average stellar population. Thus, the broadening of the absorption lines is explained completely in terms of stellar orbital motions. However, a large fraction of the stars in a galaxy are members of a binary (or even multiple) system. Stars in binary systems orbit the center of mass of the two stars and this extra velocity adds to the velocity dispersion of the galaxy. Hence, the measured kinematics of galaxies are not independent of the population of binary stars.

Previous authors have used Monte Carlo simulations to estimate the influence of binaries on the observed velocity dispersion (see Hargreaves *et al.* (1996) and references therein). This work focused mainly on observations of dwarf galaxies in the Local Group or globular clusters that can be resolved into individual stars. For a sample of stars in a galaxy, radial velocities are measured and from these velocities, the mean velocity and velocity dispersion profiles can be established. The Monte Carlo calculations by construction are very suited to interpret these “discrete” data, e.g. it is possible to check the effect of repeated observations to weed out short-period binaries. The crowded inner regions of globulars or dwarf galaxies outside of the Local Group however are impervious to this kind of study. There, integrated-light spectra are needed to measure the kinematics. As bigger telescopes make it possible to penetrate to ever lower levels of surface brightness and hence to study low-mass stellar systems at large distances, it is important to investigate the effect of binary stars on the derived LOSVD. Since Monte Carlo calculations at present are unable to yield the full LOSVD or even higher order moments such as the kurtosis without excessive computational effort, they cannot be

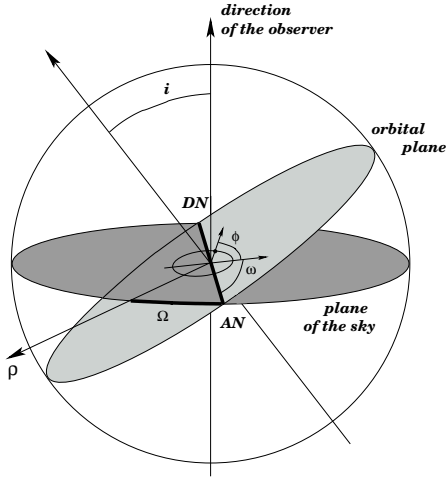


Figure 1. The orbit of the primary around the binary’s center of mass. Indicated are the descending node DN and the ascending node AN , the longitude of ascending node Ω with respect to some reference direction ρ , the argument of the periastron ω , the true anomaly ϕ and the inclination i .

employed in this context. Hence, we give analytical expressions for the velocity moments of the binary stars and for the LOSVD itself (approximating all binaries to consist of stars on circular orbits).

2 DEFINITIONS

We first give a number of definitions of important quantities and clarify some notations. We focus our attention on a single binary system. One star, the “primary”, has a mass M and the other, the “secondary” has a mass m . All orbital parameters pertain to the primary’s orbit :

- v_p : the velocity of the primary with respect to the binary’s center of mass, projected onto the observer’s line of sight

- μ_p : the gravitational constant of force for the primary’s orbit around the center of mass. If $\mu = G(m + M)$ is the force constant of the orbit relative to the secondary, then

$$\mu_p = \left(\frac{m}{m+M}\right)^3 \mu = G \frac{m^3}{(m+M)^2}. \quad (1)$$

- a_p : semi-major axis of the primary’s orbit with respect to the binary’s center of mass. If a is the semi-major axis of the primary’s orbit with respect to the secondary, then

$$a_p = \left(\frac{m}{m+M}\right) a. \quad (2)$$

- $T, e, i, \omega, \Omega, :$ respectively the period, eccentricity, inclination, argument of periastron and longitude of ascending node of the primary’s orbit. The latter does not affect the primary’s position projected onto the line of sight nor its line-of-sight velocity and hence does not enter the calculations.

- ϕ : the true anomaly along the primary’s orbit.

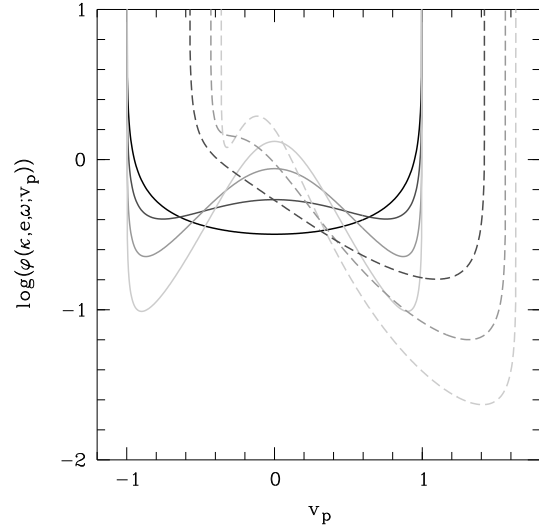


Figure 2. The specific binary LOSVD $\varphi(\kappa, e, \omega; v_p)$. In full lines, the LOSVD is plotted for $\omega = 90^\circ$ and $e = 0$ (black), $e = 0.6$ (dark grey), $e = 0.8$ (grey) and $e = 0.9$ (light grey). The other parameters are set by the choice $\kappa = 1$. In dashed lines, the LOSVD is plotted for $\omega = 45^\circ$ and the same eccentricities.

3 THE SPECIFIC BINARY LOSVD

The specific binary LOSVD gives the probability of finding the primary star with mass M with a line-of-sight velocity in the interval $[v_p - \Delta v_p/2, v_p + \Delta v_p/2]$, given that it revolves around a secondary star with mass m on an elliptical orbit with orbital parameters a, e, ω and i . Intuitively, this probability is proportional to the fraction of its period during which the primary has a velocity in this interval. Mathematically, this translates into the following expression for the specific binary LOSVD :

$$\varphi(\kappa, e, \omega; v_p) dv_p = \frac{1}{T} \frac{dv_p}{\left| \frac{dv_p}{dt} \right|}. \quad (3)$$

with v_p the line-of-sight velocity of the primary at phase angle ϕ on its orbit

$$v_p = \kappa(e \cos \omega + \cos(\phi + \omega)). \quad (4)$$

Here,

$$\kappa = \frac{2\pi a_p \sin i}{T\sqrt{1-e^2}} = \sqrt{\frac{\mu_p}{a_p}} \frac{\sin i}{\sqrt{1-e^2}}. \quad (5)$$

Hence, it follows that

$$\left| \frac{dv_p}{dt} \right| = \frac{2\pi\kappa}{(1-e^2)^{3/2}T} |\sin(\phi + \omega)| (1 + e \cos \phi)^2 \quad (6)$$

and consequently

$$\varphi(\kappa, e, \omega; v_p) = \frac{(1-e^2)^{3/2}}{2\pi\kappa} \frac{1}{|\sin(\phi + \omega)| (1 + e \cos \phi)^2}. \quad (7)$$

The specific binary LOSVD is a function solely of v_p . To eliminate the phase angle ϕ from this expression, equation (4) must be inverted :

$$\cos(\phi + \omega) = \frac{v_p}{\kappa} - e \cos \omega. \quad (8)$$

Depending on the sign of $\sin(\phi + \omega)$, there are two solutions, φ_+ and φ_- :

$$\varphi_{\pm}(\kappa, e, \omega; v_p) = \frac{1}{2\pi\kappa} \frac{(1 - e^2)^{3/2}}{\sqrt{1 - \mathcal{V}^2}} \times \left(1 + e\mathcal{V} \cos \omega \pm e\sqrt{1 - \mathcal{V}^2} \sin \omega\right)^{-2} \quad (9)$$

with $\mathcal{V} = v_p/\kappa - e \cos \omega$. This is a consequence of the fact that a star on an elliptical orbit will obtain the projected velocity v_p twice during each revolution. The LOSVD is then just the sum of φ_+ and φ_- :

$$\varphi(\kappa, e, \omega; v_p) = \frac{1}{\pi\kappa} \frac{(1 - e^2)^{3/2}}{\sqrt{1 - \mathcal{V}^2}} \times \frac{1 + e^2 \sin^2 \omega + 2e\mathcal{V} \cos \omega + e^2 \mathcal{V}^2 \cos(2\omega)}{(1 - e^2 \sin^2 \omega + 2e\mathcal{V} \cos \omega + e^2 \mathcal{V}^2)^2}. \quad (10)$$

In the case of a circular orbit – i.e. $e = 0$ – this reduces to the simple expression

$$\varphi(\kappa; v_p) = \frac{1}{\pi\kappa} \frac{1}{\sqrt{1 - \left(\frac{v_p}{\kappa}\right)^2}}, \quad (11)$$

the LOSVD of a harmonic oscillator. The specific binary LOSVD is presented for various values of ω and e in Figure 2. The LOSVD is high around the extreme velocities where $dv_p/dt = 0$ (i.e. around $v_p = \kappa(\pm 1 + e \cos \omega)$) and around the apocenter velocity $v_p = (e - 1)\kappa \cos \omega$, a direct corollary of Kepler’s second law.

4 THE VELOCITY MOMENTS OF THE SPECIFIC BINARY LOSVD

The n^{th} velocity moment of the specific binary LOSVD is defined as

$$\begin{aligned} \mu_n &= \int v_p^n \varphi(v_p) dv_p = \frac{1}{T} \int_0^T v_p^n dt \\ &= \frac{\kappa^n}{2\pi} (1 - e^2)^{3/2} \int_0^{2\pi} \frac{(\cos(\phi + \omega) + e \cos \omega)^n}{(1 + e \cos \phi)^2} d\phi. \end{aligned} \quad (12)$$

All powers in the integrand can be expanded, yielding

$$\begin{aligned} \mu_n &= \frac{\kappa^n}{2\pi} (1 - e^2)^{3/2} \sum_{k=0}^n \binom{n}{k} (e \cos \omega)^{n-k} \times \\ &\sum_{l=0}^k \binom{k}{l} (\cos \omega)^l (\sin \omega)^{k-l} (-1)^{k+l} \sum_{m=0}^{\infty} \binom{-2}{m} e^m \times \\ &\int_0^{2\pi} (\cos \phi)^{l+m} (\sin \phi)^{k-l} d\phi. \end{aligned} \quad (13)$$

For the integral to be non-zero, one condition is that $k - l = 2r$ with r an integer. The other condition is that $k + m - 2r$ must be even. Hence, k and m must both be either even or odd. This leads to the following expression for the n^{th} velocity moment :

$$\begin{aligned} \mu_n &= \frac{\kappa^n}{\pi} (1 - e^2)^{3/2} \sum_{k=0}^n \binom{n}{k} \times \\ &\sum_{r=0}^{[k/2]} \binom{k}{k - 2r} (\cos \omega)^{n-2r} (\sin \omega)^{2r} \times \end{aligned}$$

$$\sum_{m \geq 0}^{(k)} \binom{-2}{m} e^{m+n-k} \frac{\Gamma\left(\frac{k+m+1}{2} - r\right) \Gamma\left(r + \frac{1}{2}\right)}{\Gamma\left(\frac{k+m}{2} + 1\right)}. \quad (14)$$

Here, $[k/2]$ stands for the largest integer that is less than $k/2$ and $\sum_{m \geq 0}^{(k)}$ indicates that the summation runs only over those m that have the same parity as k . Γ is Euler’s Gamma function (see e.g. Gradshteyn & Ryzhik (1965), also for the other special functions appearing in this paper). Interchanging the summations, this expression can be rewritten in a more elegant form

$$\begin{aligned} \mu_n &= \frac{(\kappa \cos \omega)^n}{\sqrt{\pi}} (1 - e^2)^{3/2} \sum_{k=0}^n \binom{n}{k} \sum_{m \geq 0}^{(k)} \binom{-2}{m} \times \\ &e^{m+n-k} \frac{\Gamma\left(\frac{m+k+1}{2}\right)}{\Gamma\left(\frac{k+m}{2} + 1\right)} \times \\ &{}_2F_1\left(-\frac{k}{2}, \frac{1-k}{2}; \frac{1-k-m}{2}; -\tan^2 \omega\right). \end{aligned} \quad (15)$$

For $e = 0$, only the terms with $m + n - k = 0$ survive. This condition can only be satisfied for even moments and if $m = 0$ and $k = n$. Thus, if we substitute $2n$ for n , and make use of the fact that

$$\cos^{2n} \omega {}_2F_1\left(-n, \frac{1}{2} - n; \frac{1}{2} - n; -\tan^2 \omega\right) = 1, \quad (16)$$

then (15) reduces to

$$\mu_{2n} = \frac{1}{\pi} \left(\frac{\mu_p}{a_p} \sin i^2\right)^n B\left(n + \frac{1}{2}, \frac{1}{2}\right) \quad (17)$$

with B Euler’s beta function.

5 THE BINARY LOSVD FOR CIRCULAR ORBITS

The binary LOSVD $\tilde{\varphi}(M; v_p)$ gives the probability of finding the primary star with a line-of-sight velocity in the interval $[v_p - \Delta v_p/2, v_p + \Delta v_p/2]$. To obtain this quantity, the specific binary LOSVD (10) must be averaged over all orbital parameters. As the calculations for the general case are quite cumbersome, we only calculated the binary LOSVD in the approximation that the members of all binaries revolve on circular orbits. This is clearly not a very realistic assumption but it is instructive to have at least this first approximation of the LOSVD. To obtain the binary LOSVD, the specific binary LOSVD (11) must be averaged over all possible values of the inclination i , the orbital radius a_p and the secondary mass m . To do this, we have to assume distributions for each of these parameters.

The orbital planes of all binaries can be expected to be distributed randomly. Each direction of the normal of the orbital plane is then equally plausible. Using the notations of Figure 1, an elementary solid angle around the orbital plane’s normal is given by $dS = \sin i di d\Omega$. Since the direction S is uniformly distributed

$$\varphi(S) dS = \frac{1}{4\pi} dS = \frac{1}{4\pi} \sin i di d\Omega \quad (18)$$

one obtains

$$\varphi(i) = \int_0^{2\pi} \varphi(S) d\Omega = \frac{1}{2} \sin i \quad \text{with } i \in [0, \pi] \quad (19)$$

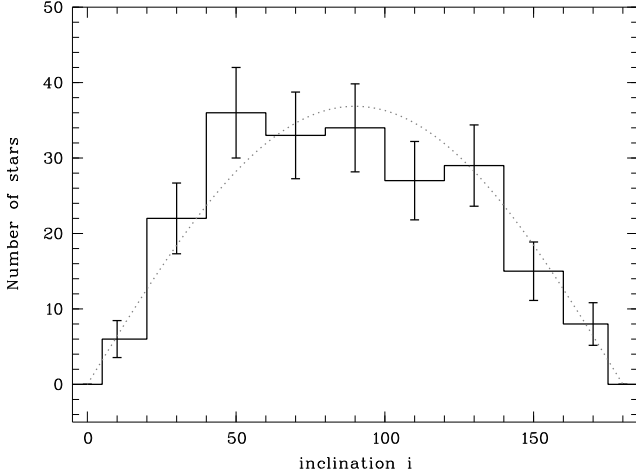


Figure 3. The distribution of the inclination i . The histogram shows the distribution extracted from Soederhjelm (1999) with the error-bars measuring the Poisson noise. Over-plotted (dotted line) is the expected distribution (19).

as the distribution of the inclination. In Soederhjelm (1999), the orbital parameters and masses of about 200 nearby visual binaries are given. The data are obtained from Hipparcos and ground-based telescopes. Figure 3 shows the distribution of the inclination, extracted from this catalog, and clearly demonstrates the validity of (19).

The distribution of the semi-major axis cannot readily be extracted from a catalog. Catalogs of visual binaries usually only contain the semi-major axis expressed in arcseconds since their distances are not known. Catalogs of spectroscopic binaries do give the semi-major axis expressed in e.g. AU but they tend to be strongly biased towards very tight binaries since these will have the highest orbital velocities and hence the largest and the easiest measurable Doppler-shifts. However, it is natural to assume that more tightly bound binaries are less easily disrupted by external influences. Hence, one would expect to observe less binaries with lower binding energies. We therefore adopt

$$\begin{aligned} \varphi(a) da &\propto E^\gamma \\ &= \frac{1-\gamma}{r_{\max}^{1-\gamma} - r_{\min}^{1-\gamma}} a^{-\gamma} da \end{aligned} \quad (20)$$

as the distribution of a (the orbital radius with respect to the secondary). Here, E is the binary's binding energy and γ is a real number. The closest gravitational few-body system at hand, our planetary system, obeys (20) quite well with $\gamma \approx 1$.

The upper and lower bounds for a , r_{\min} and r_{\max} respectively, can be estimated as follows. For a binary to be stable, the mutual gravitational attraction between its members should overcome the tidal forces exerted by the host galaxy. In other words, if we denote the average mass of a star by \bar{m} :

$$\frac{\bar{m}}{a^3} \geq \frac{2M(r)}{r^3} \quad (21)$$

with r the distance of the binary to the galaxy's center and $M(r)$ the total mass inside a sphere with radius r . This leads to the following expression for the maximum orbital radius:

$$r_{\max} \approx \sqrt[3]{\frac{3}{8\pi\bar{m}}} \quad (22)$$

with \bar{m} the average number density of the stars inside the radius r . For reasonable values of \bar{m} , r_{\max} is very large. For instance, $\bar{m} = 1 \text{ pc}^{-3}$ leads to $r_{\max} \approx 10^5 \text{ AU}$. Binaries can also be disrupted by an encounter with a third star. For typical number densities, stars approach each other to about 1500 AU once in a Hubble time as they orbit in a galaxy's gravitational potential well. Of course, not every such an encounter necessarily breaks up a binary pair. Hence, r_{\max} is at least a couple of thousand AU and can be as large as 100,000 AU. Our results turn out to be rather insensitive to the value of r_{\max} .

If the members of a binary are very close together, one of them can be in the other's Roche lobe and be disrupted by tidal and centrifugal forces. Back-of-the-envelope calculations based on typical masses and radii of K-giants (with a mass around $1 M_\odot$ and a radius of approximately $10 R_\odot$) – which one is most likely to observe since they are so luminous – give $r_{\min} \approx 15 R_\odot$ as a fair mean value.

Due to (2), the distribution of a_p is

$$\varphi(a_p) da_p = \frac{1-\gamma}{a_M^{1-\gamma} - a_m^{1-\gamma}} a_p^{-\gamma} da_p \quad (23)$$

with $a_m = m/(m+M)r_{\min}$ and analogously for a_M .

For the distribution of the secondary mass, we take the Salpeter initial mass function

$$\varphi(m) dm = \frac{1-x}{m_2^{1-x} - m_1^{1-x}} m^{-x} dm \quad (24)$$

with $x = 2.35$. The lower bound for the mass distribution is taken to be $m_1 = 0.08 M_\odot$, the mass of the most lightweight stars capable of nuclear fusion. The upper bound m_2 is treated as a free parameter of the binary orbital distribution. Realistic values for m_2 are around $1.25 M_\odot$. This corresponds to stars with a total life-time of 5-6 Gyr, comparable to the ages of the stellar populations in Local Group dwarf galaxies (e.g. Smecker-Hane *et al.* (1994)). These distributions can be compared to those found by Duquennoy & Mayor (1991) for a sample of 164 solar-type stars in the solar neighborhood. For their sample, they find the following distribution of the binary periods:

$$\varphi(\log T) d\log T \propto \exp\left(-\frac{1}{2} \left(\frac{\log T - \overline{\log T}}{\sigma_{\log T}}\right)^2\right) d\log T \quad (25)$$

with $\overline{\log T} = 4.8$ and $\sigma_{\log T} = 2.3$ (T is expressed in days). Periods were found to lie in the range $-1 < \log T < 10$. Using (20), (24) and $r_{\max} \approx 100,000 \text{ AU}$ (applicable if binaries are disrupted by tidal forces exerted by the host galaxy), we find an approximately uniform distribution of $\log T$ in the range $0 < \log T < 10$. Using $r_{\max} \approx 2000 \text{ AU}$ (applicable if binaries are disrupted by a close encounter with a third star), yields an approximately uniform distribution of $\log T$ in the range $0 < \log T < 7.5$. As always, the truth lies somewhere in between these two extremes. The Salpeter law adopted here provides a reasonable fit to the mass-ratio distribution although it over-estimates the number of low-mass companions with $q < 0.4$ found by Duquennoy & Mayor.

We start with the integration of the specific binary LOSVD (11) over the inclination, making use of the distribution (19). The integration region must be limited to

$$\arcsin t_0 < i < \pi - \arcsin t_0 \quad (26)$$

with $t_0 = \sqrt{\frac{a_p v_p}{\mu_p}}$, to assure that the argument of the square root in the denominator of (11) is positive. This, of course, is because, for a given a_p and μ_p , some binaries with a large inclination cannot reach the velocity v_p and must be excluded from the integration. The binary LOSVD after this integration becomes

$$\begin{aligned} \tilde{\varphi}(M; v_p) &= \frac{1}{2\pi v_p} \int_{\arcsin t_0}^{\pi - \arcsin t_0} \frac{\sin i}{\sqrt{\frac{1}{t_0^2} \sin^2 i - 1}} di \\ &= \frac{1}{2} \sqrt{\frac{a_p}{\mu_p}}. \end{aligned} \quad (27)$$

We employ the distribution function (23) to average formula (27) over the semi-major axis. The integration region is now limited to

$$a_m < a_p < \min\left(a_M, \frac{\mu_p}{v_p^2}\right). \quad (28)$$

This ensures the positivity of the binary LOSVD by excluding all binaries that, for a given μ_p , cannot reach the velocity v_p . The binary LOSVD at this stage of the integrations takes the form

$$\begin{aligned} \tilde{\varphi}(M; v_p) &= \frac{1-\gamma}{3-2\gamma} \frac{1}{r_{\max}^{1-\gamma} - r_{\min}^{1-\gamma}} \frac{1}{\sqrt{G}} m^{\gamma-5/2} (m+M)^{2-\gamma} \times \\ &\quad \left[\left(\min\left(a_M, \frac{\mu_p}{v_p^2}\right) \right)^{\frac{3}{2}-\gamma} - a_m^{\frac{3}{2}-\gamma} \right]. \end{aligned} \quad (29)$$

The condition $a_M \leq \frac{\mu_p}{v_p^2}$ is satisfied if

$$m \geq m_0 = \frac{M}{2} \left(\frac{r_{\max} v_p^2}{GM} + \sqrt{\frac{r_{\max} v_p^2}{GM} \left(4 + \frac{r_{\max} v_p^2}{GM}\right)} \right). \quad (30)$$

In that case, there is no danger of the integrand becoming negative. If $m < m_0$ however, the integration region must be limited to

$$m \geq m_3 = \frac{M}{2} \left(\frac{r_{\min} v_p^2}{GM} + \sqrt{\frac{r_{\min} v_p^2}{GM} \left(4 + \frac{r_{\min} v_p^2}{GM}\right)} \right) \quad (31)$$

if $\gamma < 3/2$. Clearly, $m_3 \ll m_0$ if $v_p > 0$. The integration over the secondary mass involves three basic integrals. The first one is

$$\begin{aligned} \mathcal{I}_1(x_1, x_2) &= \frac{1-\gamma}{3-2\gamma} \frac{r_{\max}^{3/2-\gamma}}{r_{\max}^{1-\gamma} - r_{\min}^{1-\gamma}} \frac{1}{\sqrt{G}} \frac{1-x}{m_2^{1-x} - m_1^{1-x}} \times \\ &\quad \int_{x_1 M}^{x_2 M} m^{-x-1} (m+M)^{1/2} dm \\ &= \frac{1-\gamma}{3-2\gamma} \frac{r_{\max}^{3/2-\gamma}}{r_{\max}^{1-\gamma} - r_{\min}^{1-\gamma}} \frac{1}{\sqrt{G}} \frac{1-x}{m_2^{1-x} - m_1^{1-x}} \times \\ &\quad M^{1/2-x} F\left(-x-1, \frac{1}{2}; x_1, x_2\right). \end{aligned} \quad (32)$$

with

$$\begin{aligned} \mathcal{F}(a, b; x_1, x_2) &= \int_{x_1}^{x_2} x^a (1+x)^b dx, \quad x_1 < x_2 \\ &= \mathcal{F}(a, b; x_1, x_2) \quad \text{if } x_2 \leq 1 \\ &= \mathcal{F}(a, b; x_1, 1) + \end{aligned}$$

$$\begin{aligned} &\mathcal{F}\left(-a-b-2, b; \frac{1}{x_2}, 1\right) \\ &\quad \text{if } x_2 > 1 \text{ but } x_1 \leq 1 \\ &= \mathcal{F}\left(-a-b-2, b; \frac{1}{x_2}, \frac{1}{x_1}\right) \\ &\quad \text{if } x_2 > 1 \text{ and } x_1 > 1 \end{aligned} \quad (33)$$

and

$$\begin{aligned} \mathcal{F}(a, b; x_1, x_2) &= \frac{x_2^{a+1}}{a+1} {}_2F_1(-b, 1+a; 2+a; -x_2) \\ &\quad - \frac{x_1^{a+1}}{a+1} {}_2F_1(-b, 1+a; 2+a; -x_1). \end{aligned} \quad (34)$$

Here, ${}_2F_1$ is the hypergeometric function. The second integral is completely analogous :

$$\begin{aligned} \mathcal{I}_2(x_1, x_2) &= -\frac{1-\gamma}{3-2\gamma} \frac{r_{\min}^{3/2-\gamma}}{r_{\max}^{1-\gamma} - r_{\min}^{1-\gamma}} \frac{1}{\sqrt{G}} \frac{1-x}{m_2^{1-x} - m_1^{1-x}} \times \\ &\quad \int_{x_1 M}^{x_2 M} m^{-x-1} (m+M)^{1/2} dm \\ &= -\frac{1-\gamma}{3-2\gamma} \frac{r_{\min}^{3/2-\gamma}}{r_{\max}^{1-\gamma} - r_{\min}^{1-\gamma}} \frac{1}{\sqrt{G}} \frac{1-x}{m_2^{1-x} - m_1^{1-x}} \times \\ &\quad M^{1/2-x} F\left(-x-1, \frac{1}{2}; x_1, x_2\right). \end{aligned} \quad (35)$$

The third basic integral is

$$\begin{aligned} \mathcal{I}_3(v_p, x_1, x_2) &= \frac{1-\gamma}{3-2\gamma} \frac{1}{r_{\max}^{1-\gamma} - r_{\min}^{1-\gamma}} \frac{1-x}{m_2^{1-x} - m_1^{1-x}} \times \\ &\quad \frac{1}{\sqrt{G}} \left(\frac{GM}{v_p^2}\right)^{3/2-\gamma} \int_{x_1 M}^{x_2 M} m^{-2\gamma-x+2} (m+M)^{\gamma-1} dm \\ &= \frac{1-\gamma}{3-2\gamma} \frac{1}{r_{\max}^{1-\gamma} - r_{\min}^{1-\gamma}} \frac{1-x}{m_2^{1-x} - m_1^{1-x}} \times \\ &\quad \frac{M^{1/2-x}}{\sqrt{G}} \left(\frac{GM}{v_p^2}\right)^{3/2-\gamma} F(-2\gamma-x+2, \gamma-1; x_1, x_2). \end{aligned} \quad (36)$$

In each of these integrals, the factor

$$\mathcal{Q} = \frac{1-\gamma}{3-2\gamma} \frac{1}{r_{\max}^{1-\gamma} - r_{\min}^{1-\gamma}} \frac{M^{1/2-x}}{\sqrt{G}} \frac{1-x}{m_2^{1-x} - m_1^{1-x}} \quad (37)$$

can be taken out. We are then left with the following three building blocks :

$$\begin{aligned} \mathcal{I}_1(x_1, x_2) &= r_{\max}^{3/2-\gamma} F\left(-x-1, \frac{1}{2}; x_1, x_2\right), \\ \mathcal{I}_2(x_1, x_2) &= -r_{\min}^{3/2-\gamma} F\left(-x-1, \frac{1}{2}; x_1, x_2\right), \\ \mathcal{I}_3(v_p, x_1, x_2) &= \left(\frac{GM}{v_p^2}\right)^{3/2-\gamma} \times \\ &\quad F(-2\gamma-x+2, \gamma-1; x_1, x_2). \end{aligned} \quad (38)$$

The binary LOSVD, averaged over all orbital parameters, finally takes the following form :

$$\begin{aligned} \tilde{\varphi}(M; v_p) &= \mathcal{Q} \left[\mathcal{I}_1\left(\max\left\{\frac{m_1}{M}, \frac{m_0}{M}\right\}, \frac{m_2}{M}\right) + \right. \\ &\quad \mathcal{I}_2\left(\max\left\{\frac{m_3}{M}, \frac{m_1}{M}\right\}, \frac{m_2}{M}\right) + \\ &\quad \left. \mathcal{I}_3\left(v_p, \max\left\{\frac{m_3}{M}, \frac{m_1}{M}\right\}, \min\left\{\frac{m_2}{M}, \frac{m_0}{M}\right\}\right) \right]. \end{aligned} \quad (39)$$

As can be expected, the LOSVD goes to zero for $m_3 \geq m_2$ or equivalently for

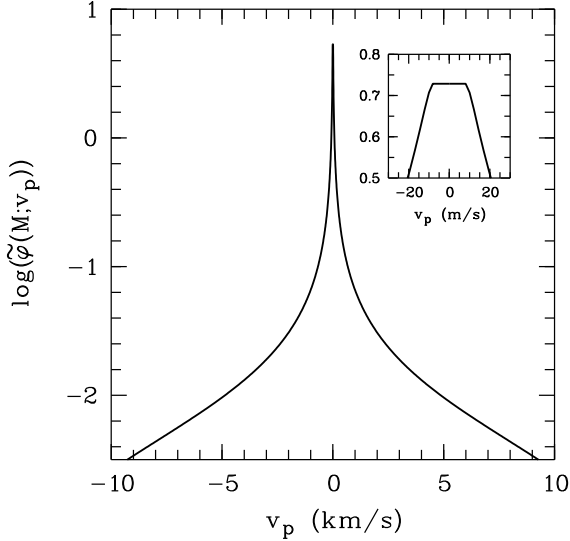


Figure 4. The logarithm of the binary LOSVD $\tilde{\varphi}(M; v_p)$ for circular orbits. The primary mass is $M = 0.8 M_\odot$, the secondary mass is averaged over the interval $0.08 - 1.5 M_\odot$, $r_{\min} = 15 R_\odot$, $r_{\max} = 101559.1 \text{ AU} \approx 0.5 \text{ pc}$ ($\bar{n} = 1 \text{ pc}^{-3}$), $\gamma = 1$ and $x = 2.35$. The inset shows the flat top of the LOSVD for very small velocities. For the parameter values adopted here, the LOSVD is constant for velocities smaller than $v_1 \approx 7 \text{ m/s}$.

$$v_p \geq v_3 = \sqrt{\frac{Gm_2^2}{(m_2 + M)r_{\min}}}, \quad (40)$$

the highest line-of-sight velocity any binary can reach. As long as $m_0 < m_1$, or equivalently for

$$v_p \leq v_1 = \sqrt{\frac{Gm_1^2}{(m_1 + M)r_{\max}}}, \quad (41)$$

the LOSVD is velocity independent. This is the highest velocity that the slowest binaries, i.e. the ones with the lowest secondary mass and the largest orbital radius, can reach. Usually, r_{\max} is very large and consequently, v_1 will be a very small velocity, of the order of a few m/s (see Figure 4).

To be exact, the binary LOSVD (39) still needs to be multiplied with the probability that the primary star is actually observed and then be averaged over the primary mass. It is this final function that quantifies the extra broadening of the absorption lines due to the binary population. However, the probability of observing a star of a particular spectral type depends both on its intrinsic brightness and on the number of such stars that are around. As the brightest stars are also the most scarce ones while the faintest stars are extremely abundant, this probability will be sharply peaked. For old to intermediate stellar populations, this peak corresponds to early K giants on the tip of the giant branch. We will therefore not do this last integration and instead use an average value for the primary mass. Most authors use $M = 0.8 M_\odot$ and this is the value we will adopt here.

6 THE MOMENTS OF THE BINARY LOSVD FOR NON-CIRCULAR ORBITS

The binary LOSVD for elliptic orbits is not analytically tractable, but its velocity moments, which we denote by μ_n ,

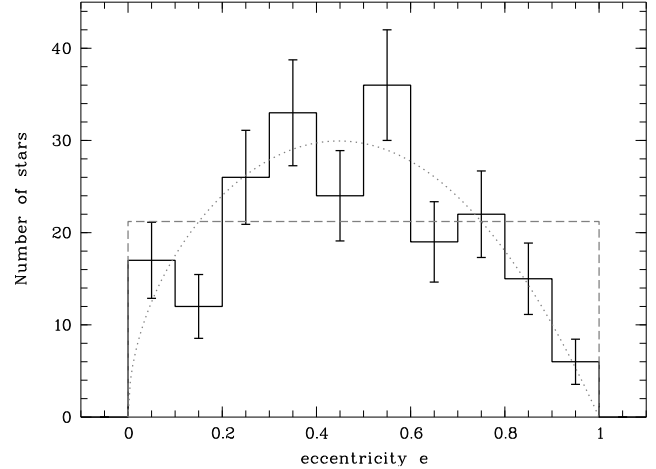


Figure 5. The distribution of the eccentricity e . The histogram shows the distribution extracted from Soederhjelm (1999) with the errorbars measuring the Poisson noise. Over-plotted in dotted lines is the distribution (43). The uniform distribution is plotted in dashed lines.

are. We set out with the expression (15) for the moments of the specific binary LOSVD and average it over the argument of the periastron ω , the inclination i , the secondary mass m , the semi-major axis a_p and the eccentricity e . For i and m , one can use the distributions (19) and (24). The distribution (23) for the semi-major axis is also still applicable but care has to be taken with the integration limits: the bounds for a_p are set by the conditions

$$\begin{aligned} a(1+e) &\leq r_{\max}, \\ a(1-e) &\geq r_{\min}, \end{aligned} \quad (42)$$

which makes the integration limits of a_p dependent of e .

As can be seen in Figure 5, the distribution of the eccentricity of a sample of 200 visual binaries can be approximated fairly accurately by

$$\varphi(e) de = \frac{(1+\alpha)e^\alpha(1-e^2)^\beta}{e_{\max}^{\alpha+1} {}_2F_1\left(-\beta, \frac{1+\alpha}{2}; \frac{3+\alpha}{2}; e_{\max}^2\right)} de \quad (43)$$

with $\alpha = 0.5$, $\beta = 1$ and maximum eccentricity $e_{\max} = 1$. The eccentricity distribution found by Duquenooy & Mayor (1991) shows that tight binaries have more circular orbits than wide ones but, overall, their eccentricity distribution is similar to the one derived by Soederhjelm. In the remainder, we consider the parameters α , β and e_{\max} to be fixed by the observations. This distribution reaches a maximum for

$$e_{\text{top}} = \sqrt{\frac{\alpha}{2\beta + \alpha}} \approx 0.45, \quad (44)$$

for the parameter values adopted here. The uniform distribution $\varphi(e) = 1/e_{\max}$, which is the distribution advocated by Hargreaves *et al.* (1996) and Mateo *et al.* (1993), is obtained by setting $\alpha = \beta = 0$.

The argument of the periastron ω is obviously distributed randomly between $\omega = 0$ and $\omega = 2\pi$. Therefore,

$$\varphi(\omega) d\omega = \frac{1}{2\pi} d\omega. \quad (45)$$

Averaging the n^{th} velocity moment of the specific binary LOSVD (15) over ω involves the integral

$$\frac{1}{2\pi} \int_0^{2\pi} (\cos \omega)^{n-2r} (\sin \omega)^{2r} d\omega \quad (46)$$

which can only be non-zero if n is even. We will therefore consider only the even moments and make the transformation $n \rightarrow 2n$ in which case

$$\frac{1}{2\pi} \int_0^{2\pi} (\cos \omega)^{2n-2r} (\sin \omega)^{2r} d\omega = \frac{1}{\pi} \frac{\Gamma(n-r+1/2)\Gamma(r+1/2)}{\Gamma(n+1)}. \quad (47)$$

The integrations over i and m are pretty straightforward and one obtains the following expression for the moments $\tilde{\mu}_{2n}$:

$$\begin{aligned} \tilde{\mu}_{2n} &= \left(\frac{GM}{a}\right)^n \frac{1}{(2n+1)\sqrt{\pi}} \frac{1-x}{\left(\frac{m_2}{M}\right)^{1-x} - \left(\frac{m_1}{M}\right)^{1-x}} \times \\ &F\left(2n-x, -n, \frac{m_1}{M}; \frac{m_2}{M}\right) \sum_{k=0}^{2n} \binom{2n}{k} \sum_{m \geq 0}^{(k)} \binom{-2}{m} \times \\ &e^{m+2n-k} (1-e^2)^{3/2-n} \frac{\Gamma\left(\frac{m+k+1}{2}\right)}{\Gamma\left(\frac{k+m}{2}+1\right)} \times \\ &{}_3F_2\left(-\frac{k}{2}, \frac{1-k}{2}, \frac{1}{2}; \frac{1-k-m}{2}, \frac{1}{2} - n; 1\right). \end{aligned} \quad (48)$$

The next step is the integration over the semi-major axis a , making use of (20):

$$\frac{1-\gamma}{r_{\max}^{1-\gamma} - r_{\min}^{1-\gamma}} \int_{\frac{r_{\min}}{1+e}}^{\frac{r_{\max}}{1+e}} a^{-\gamma-n} da = \frac{1-\gamma}{1-\gamma-i} \frac{1}{r_{\max}^{1-\gamma} - r_{\min}^{1-\gamma}} \times \left[\left(\frac{r_{\max}}{1+e}\right)^{1-\gamma-n} - \left(\frac{r_{\min}}{1+e}\right)^{1-\gamma-n} \right]. \quad (49)$$

Finally, we are left with the integration over all possible values of the eccentricity. Making use of the lemma

$$\begin{aligned} \mathcal{G}(a, b, c; x) &= \int_0^x y^a (1+y)^b (1-y)^c dy \\ &= \frac{x^{a+1}}{a+1} \sum_{m=0}^{\infty} \frac{(-b)_m (a+1)_m}{(a+2)_m m!} (-x)^m \times \\ &{}_2F_1(-c, a+m+1; a+m+2; x) \end{aligned} \quad (50)$$

one finds that:

$$\begin{aligned} \tilde{\mu}_{2n} &= \frac{(GM)^n}{\sqrt{\pi}} \frac{(1-\gamma)(1-x)}{(1-\gamma-n)(2n+1)} \frac{1}{r_{\max}^{1-\gamma} - r_{\min}^{1-\gamma}} \times \\ &\frac{1}{\left(\frac{m_2}{M}\right)^{1-x} - \left(\frac{m_1}{M}\right)^{1-x}} \frac{1+\alpha}{e_{\max}^{\alpha+1} {}_2F_1\left(-\beta, \frac{1+\alpha}{2}; \frac{3+\alpha}{2}; e_{\max}^2\right)} \times \\ &F\left(2n-x, -n; \frac{m_1}{M}, \frac{m_2}{M}\right) \times \\ &\sum_{k=0}^{2n} \binom{2n}{k} \sum_{m \geq 0}^{(k)} \binom{-2}{m} \frac{\Gamma\left(\frac{m+k+1}{2}\right)}{\Gamma\left(\frac{k+m}{2}+1\right)} \times \\ &{}_3F_2\left(-\frac{k}{2}, \frac{1-k}{2}, \frac{1}{2}; \frac{1-k-m}{2}, \frac{1}{2} - n; 1\right) \times \\ &\left[r_{\max}^{1-\gamma-n} \mathcal{G}\left(m+2n-k+\alpha, \frac{1}{2} + \gamma + \beta, \frac{3}{2} - n + \beta; e_{\max}\right) \right. \\ &\left. - r_{\min}^{1-\gamma-n} \mathcal{G}\left(m+2n-k+\alpha, \frac{3}{2} - n + \beta, \right) \right] \end{aligned}$$

$$\left. \frac{1}{2} + \gamma + \beta; e_{\max} \right)]. \quad (51)$$

For $e_{\max} = 0$, only the terms with $m+2n-k=0$ survive. This is only possible if $m=0$ and $k=2n$ and (51) reduces to

$$\tilde{\mu}_{2n} = \frac{(GM)^n}{2n+1} \frac{1-\gamma}{1-\gamma-n} \frac{r_{\max}^{1-\gamma-n} - r_{\min}^{1-\gamma-n}}{r_{\max}^{1-\gamma} - r_{\min}^{1-\gamma}} \times \frac{1-x}{\left(\frac{m_2}{M}\right)^{1-x} - \left(\frac{m_1}{M}\right)^{1-x}} F\left(2n-x, -n; \frac{m_1}{M}, \frac{m_2}{M}\right), \quad (52)$$

the expression for the moments of the LOSVD for circular orbits.

In the next paragraph, we discuss how the velocity dispersion of the binary LOSVD for non-circular orbits depends on the distributions of the different orbital parameters. Another important point that will be addressed is the way the shape of the observed LOSVD depends on the binary fraction.

7 DISCUSSION

7.1 The binary velocity dispersion as a function of the orbital parameters

As is obvious from Figures 6 to 10, the binary velocity dispersion, i.e. the second order velocity moment $\tilde{\mu}_2$, depends most sensitively on the inner cutoff radius r_{\min} and the exponent γ in the distribution of the semi-major axis a_p and to a lesser degree on the primary mass M and the exponent x in the Salpeter IMF adopted as the distribution of the secondary mass m_2 . As the stars in a binary system are allowed to approach each other more closely – in other words, as r_{\min} is lowered – their orbital velocities rise rapidly, boosting the velocity dispersion of the binary population as a whole to values as high as 10 km/s for $r_{\min} = 1 R_{\odot}$, as can be seen in Figure 6. Since the bright giant stars that one is most likely to observe have radii of the order of 10 R_{\odot} , the velocity dispersion is limited to values below 4 km/s. The value of the outer cut-off radius, r_{\max} , does not strongly affect the value of the binary dispersion. Higher r_{\max} values mean that more stars orbit on wide and consequently slow orbits, causing the dispersion to be a bit lower. A higher value of γ causes stars to move on more tightly bound orbits, thus boosting their velocities. This is clear from Figure 10. If x , the exponent of the Salpeter IMF, is made larger, the secondary masses will tend to be lower which also causes the primary's orbital velocity and hence the velocity dispersion of the binary population as a whole to be lower (see Figure 11). If M is raised, the center of mass will be closer to the primary, causing its orbital velocity to drop slowly, as is observed in Figure 8. Larger values for m_2 will produce heavier secondary stars. A slowly rising velocity dispersion ensues, as can be seen in Figure 9. The same exercise was done with a uniform distribution for the eccentricity. The outcome was essentially identical: the binary velocity dispersion differed at most by 0.1 km/s. Hence, our results do not depend critically on the adopted distribution for the eccentricity.

The values for the binary velocity dispersion obtained here are about the same as those obtained by Hargreaves *et al.* although these authors use Gaussian distributions for the ellipticity, secondary mass and period, making it difficult to

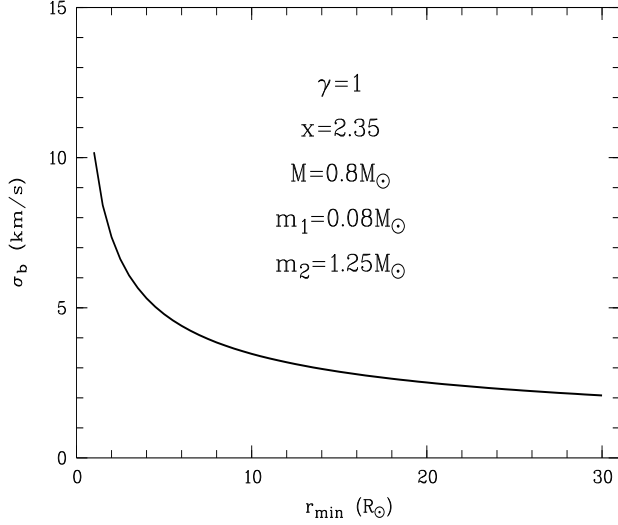


Figure 6. The binary velocity dispersion as a function of the inner cutoff radius, r_{\min} . The values of the parameters are indicated in the plot.

directly compare the results. Mateo *et al.* (1993), employing a Monte Carlo simulation with a uniformly distributed ellipticity and secondary mass and a power law distribution for the period, find higher velocity dispersions. However, it is mentioned by Hargreaves *et al.* and by Olszewski *et al.* that the values published by Mateo *et al.* are overestimated due to a coding error. The corrected Mateo *et al.* values however are in good agreement with the results obtained by other authors and with those presented here.

In the following, we will adopt the model with

$$\begin{aligned}
 \gamma &= 1 \\
 x &= 2.35 \\
 r_{\min} &= 15 R_{\odot} \\
 m_1 &= 0.08 M_{\odot} \\
 m_2 &= 1.25 M_{\odot} \\
 M &= 0.8 M_{\odot}
 \end{aligned} \tag{53}$$

as our “standard” model. Its velocity dispersion is $\sigma_b = 2.87$ km/s and its kurtosis amounts to $\xi_{4,b} = 86.89$.

7.2 The observed LOSVD

The LOSVD that would actually be observed is the convolution of the binary LOSVD (describing the motion of stars in binary systems) and the intrinsic LOSVD of the galaxy (determined by the stars’ orbital motions through the galaxy). If we denote the intrinsic galaxy LOSVD by $\varphi_i(v_p)$ and the binary LOSVD by $\varphi_b(v_p)$, then the observed LOSVD $\varphi_o(v_p)$ can be written as

$$\begin{aligned}
 \varphi_o(v_p) &= \int_{-\infty}^{+\infty} \varphi_i(v_p - x) ((1 - \alpha) \delta(x) + \alpha \varphi_b(x)) dx \\
 &= (1 - \alpha) \varphi_i(v_p) + \alpha \int \varphi_i(v_p - x) \varphi_b(x) dx
 \end{aligned} \tag{54}$$

with $\delta(x)$ the Dirac delta function and α the binary fraction, i.e. the fraction of visible (solar-mass) giant stars that have a companion. As an indication, Duquenooy & Mayor

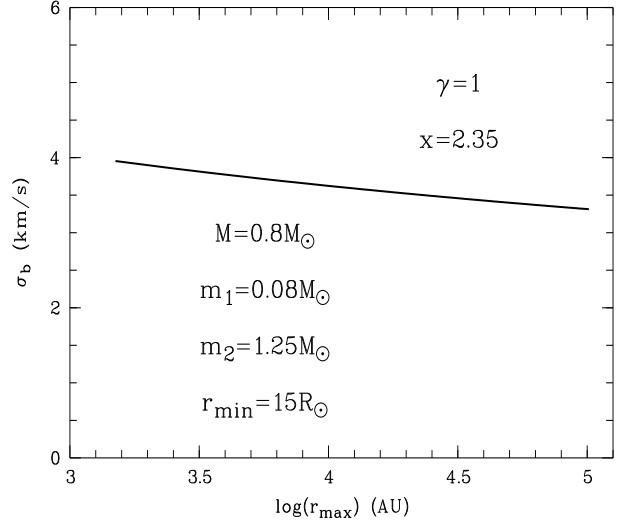


Figure 7. The binary velocity dispersion as a function of the outer cutoff radius, r_{\max} . The values of the parameters are indicated in the plot.

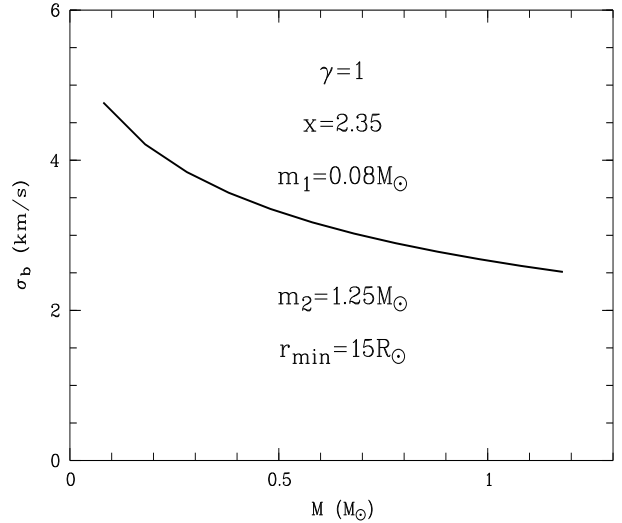


Figure 8. The binary velocity dispersion as a function of the primary mass M .

(1991) find $\alpha \approx 0.6$ for solar-mass stars in the solar neighborhood with the same range of binary periods as adopted here. In Figure 12, the observed LOSVD is plotted for different binary fractions. The intrinsic LOSVD is a Gaussian with dispersion $\sigma_i = 3$ km/s. The binary LOSVD is given by (39) with $M = 0.8 M_{\odot}$, $r_{\min} = 15 R_{\odot}$, $r_{\max} = 101559.1$ AU ($\bar{n} = 1$ pc $^{-3}$), $\gamma = 1$ and $x = 2.35$. The secondary mass is averaged over the interval $0.08 - 1.5 M_{\odot}$. The LOSVD becomes clearly more peaked and develops broader high-velocity wings as the binary fraction increases. A comprehensive way of assessing the change in the shape of the observed LOSVD as a function of the binary fraction is to study its moments. If the intrinsic galaxy LOSVD is a symmetric function of the line-of-sight velocity, then one finds for the velocity dispersion σ_o and the fourth order moment $\mu_{4,o}$ of the observed LOSVD :

$$\sigma_o^2 = \sigma_i^2 + \alpha \sigma_b^2$$

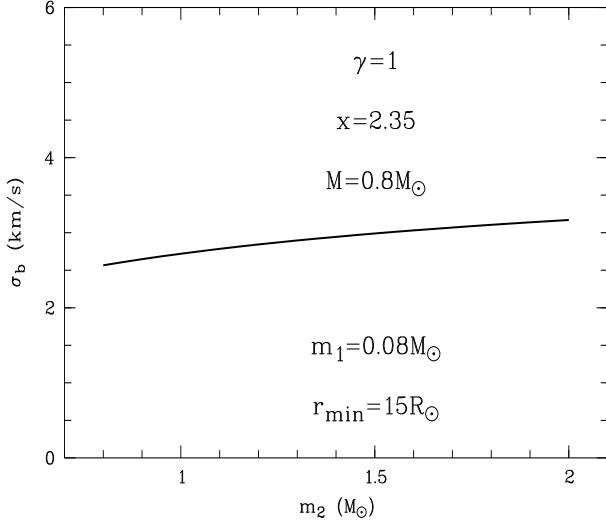


Figure 9. The binary velocity dispersion as a function of the upper mass cutoff m_2 .

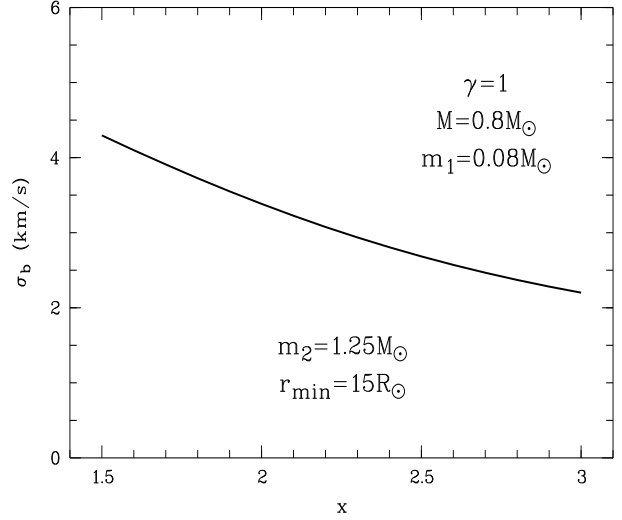


Figure 11. The binary velocity dispersion as a function of the exponent x in the Salpeter law for the secondary mass distribution.

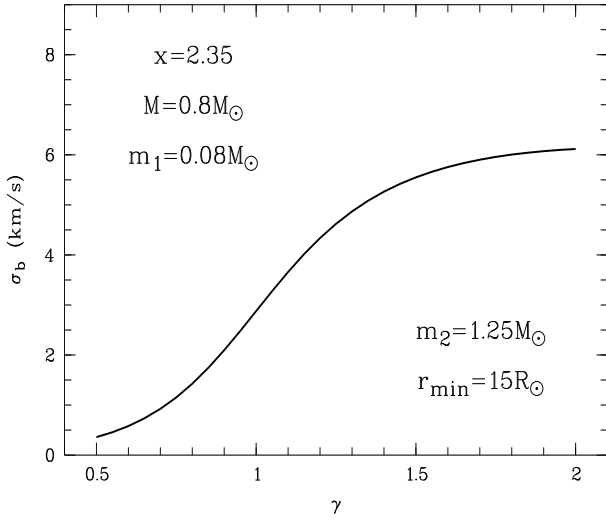


Figure 10. The binary velocity dispersion as a function of the exponent γ in the distribution of the major axis a_p .

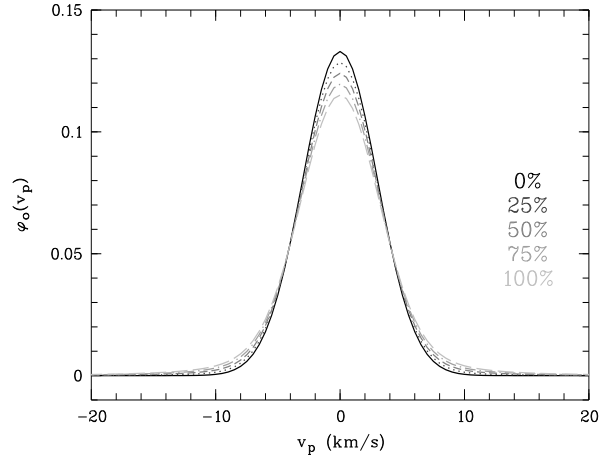


Figure 12. The observed LOSVD for different binary fractions α , indicated in the plot. The intrinsic LOSVD is a Gaussian with dispersion $\sigma_i = 3$ km/s, the binary LOSVD is given by (39) with $M = 0.8 M_\odot$, $r_{\min} = 15 R_\odot$, $r_{\max} = 101559.1$ AU ($\bar{n} = 1 \text{ pc}^{-3}$), $\gamma = 1$ and $x = 2.35$.

$$\mu_{4,o} = \mu_{4,i} + \alpha\mu_{4,b} + 6\alpha\sigma_i^2\sigma_b^2 \quad (55)$$

with σ_i^2 and $\mu_{4,i}$ respectively the second and fourth order moments of the intrinsic galaxy LOSVD and σ_b^2 and $\mu_{4,b}$ respectively the second and fourth order moments of the binary LOSVD. The fact that we have the fourth order moment of the binary LOSVD at our disposal allows us to study not only the observed velocity dispersion but also the observed LOSVD's kurtosis

$$\xi_{4,o} = \frac{\mu_{4,o}}{\sigma_o^4} \quad (56)$$

as a function of the binary fraction.

From Figures 13, 14 and 15, it is clear that the velocity dispersion of only the most light-weight galaxies will be appreciably affected by their binary population. There, the velocity dispersion of the observed LOSVD is presented as a function of the binary fraction for intrinsic Gaussian LOSVDs with $\sigma_i = 3$ km/s, $\sigma_i = 6$ km/s and $\sigma_i = 9$ km/s.

The kinematics of the binary population are those of the “standard” model. Only if the intrinsic velocity dispersion is of the same order as the binary velocity dispersion, i.e. $\sigma_i \approx 3$ km/s, is there a noticeable change in the velocity dispersion. A binary fraction of 60% raises the velocity dispersion of the $\sigma_i = 3$ km/s LOSVD with 24%, that of the $\sigma_i = 6$ km/s LOSVD with 7% and that of the $\sigma_i = 9$ km/s LOSVD with 3%. These Figures, however, yield a surprising result : whereas the influence of the binary population on the observed velocity dispersion is limited to stellar systems with intrinsic dispersions that are comparable to the binary velocity dispersion, the shape of the observed LOSVD – as quantified by the kurtosis – is appreciably affected for systems with intrinsic dispersions as high as three times that of the binaries. The kurtosis can be related to a quantity that is of more direct interest to observers : the coefficient of the fourth order term in the expansion of the LOSVD

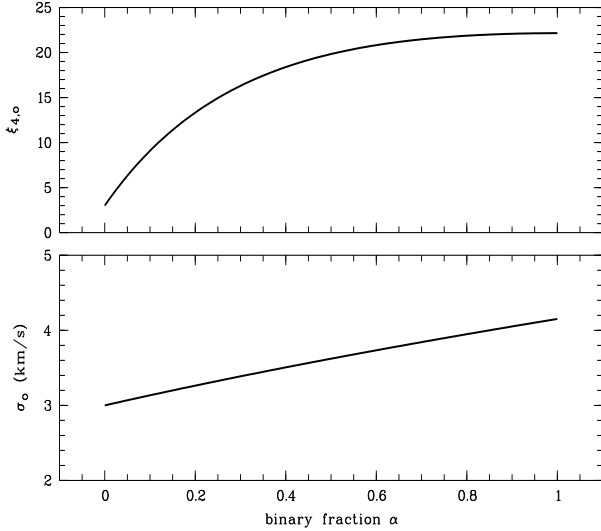


Figure 13. The velocity dispersion and kurtosis of the observed LOSVD as a function of the binary fraction α . The intrinsic galaxy LOSVDs is a Gaussian with $\sigma_i = 3$ km/s. The parameter values are those of the “standard” model, i.e. with $\sigma_b \approx 3$ km/s.

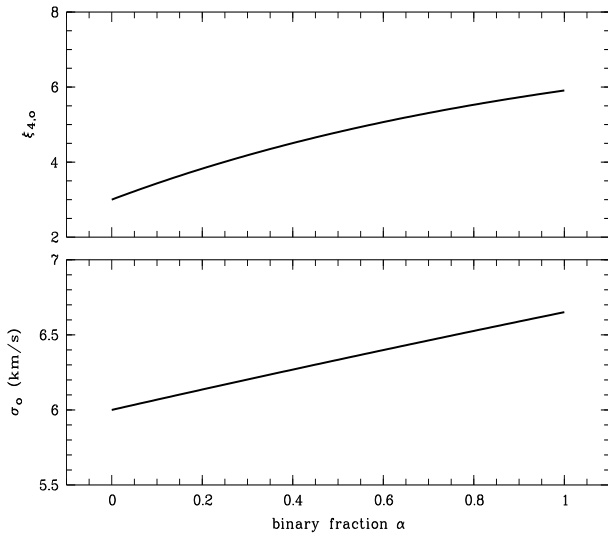


Figure 14. The velocity dispersion and kurtosis of the observed LOSVD as a function of the binary fraction α . The intrinsic galaxy LOSVDs is a Gaussian with $\sigma_i = 6$ km/s. The parameter values are those of the “standard” model, i.e. with $\sigma_b \approx 3$ km/s.

in Gauss-Hermite polynomials, h_4 (Gerhard (1993), van der Marel & Franx (1993)) :

$$h_4 \approx \frac{\xi_{4,o} - 3}{8\sqrt{6}}. \quad (57)$$

E.g. a binary fraction $\alpha = 0.6$ raises the kurtosis of a $\sigma_i = 6$ km/s Gaussian to 5.09 ($h_4 \approx 0.1$) and that of a $\sigma_i = 9$ km/s Gaussian to 3.47 ($h_4 \approx 0.025$). For stellar systems with lower intrinsic velocity dispersions, the LOSVDs will be even more distinctly non-Gaussian.

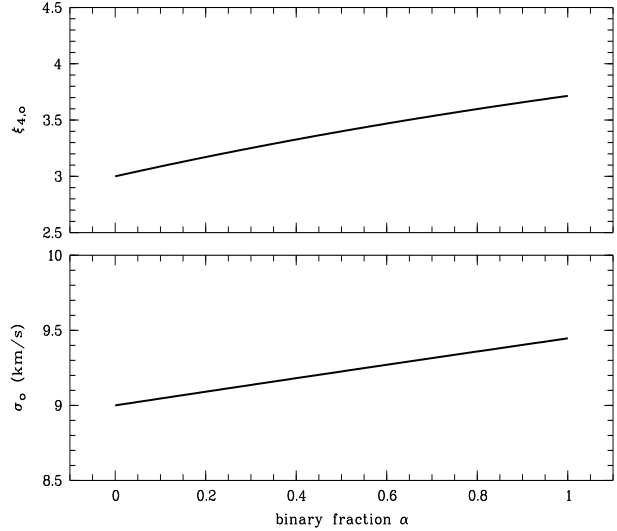


Figure 15. The velocity dispersion and kurtosis of the observed LOSVD as a function of the binary fraction α . The intrinsic galaxy LOSVDs is a Gaussian with $\sigma_i = 9$ km/s. The parameter values are those of the “standard” model, i.e. with $\sigma_b \approx 3$ km/s.

8 CONCLUSIONS

The maximum additional velocity dispersion due to binary stars is estimated at $\sigma_b \approx 3$ km/s, in good agreement with other authors. Only stellar systems with intrinsic velocity dispersions comparable to this value will have observed velocity dispersions that are noticeably affected by the presence of binaries, i.e. dwarf Spheroidals such as those found in the Local Group (Dekel & Silk (1986)), globular clusters, low-surface-brightness disk galaxies (Bottema (1993)) and the central regions of nucleated dwarf ellipticals. Not only the velocity dispersion but also the shape of the galaxy’s LOSVD is altered. The presence of binaries has a measurable effect on the kurtosis of the observed LOSVD for stellar systems with a velocity distribution as high as 10 km/s. For stellar systems with lower velocity dispersions, the LOSVDs will be even more distinctly non-Gaussian, being strongly peaked with broad wings. This feature can mimic radial anisotropy which combined with the enhanced velocity dispersion could lead to an over-estimation of the dark matter content of dSphs and globulars.

If the kinematics of a galaxy are derived from the radial velocities of discrete stars – as is the case for the dwarf spheroidals in the Local Group – repeated observations can eliminate the binaries from the star sample. Methods that rely on integrated light spectra – e.g. the crowded regions of globular clusters or dwarf galaxies outside the Local Group – will be plagued by the above mentioned effects.

REFERENCES

- Bottema R., 1993, A&A, 275, 16
- Duquennoy A. & Mayor M., 1991, A&A, 248, 485
- Dekel A. & Silk J. 1986, ApJ, 303, 39
- Gerhard O., 1993, MNRAS, 265, 213
- Gradshteyn I. S. & Ryzhik I. M., 1965, “Table of integrals, series, and products”, Academic Press, New York
- Hargreaves, J. C., Gilmore, G. & Annan J. D., 1996, MNRAS, 279, 108

- Mateo M. *et al.*, 1993, AJ, 105, 510
Olszewski E. W., Pryor C. & Armandroff T. E., 1996, AJ, 111,
750
Soederhjelm S., 1999, A&A, 341, 121
Smecker-Hane T. A. *et al.*, 1994, AJ, 108, 507
van der Marel R. P. & Franx M., 1993, ApJ, 407, 525